The Use of C-MnO2 as Hybrid Precursor Support for a Pt/C-MnxO1+x Catalyst with Enhanced Activity
for the Methanol Oxidation Reaction (MOR)

(Article begins on next page)

21 May 2025

Article

The Use of C-MnO₂ as Hybrid Precursor Support for a Pt/C-Mn$_x$O$_{1+x}$ Catalyst with Enhanced Activity for the Methanol Oxidation Reaction (MOR)

Alessandro H.A. Monteverde Videla, Luigi Osmieri, Reza Alipour Moghadam Esfahani, Juqin Zeng, Carlotta Francia and Stefania Specchia *

Department of Applied Science and Technology, Politecnico di Torino, Corso Duca degli Abruzzi 24, 10129 Torino, Italy; E-Mails: alessandro.monteverdevidela@polito.it (A.H.A.M.V.); luigi.osmieri@polito.it (L.O.); reza.alipour@polito.it (R.A.M.E.); juqin.zeng@polito.it (J.Z.); carlotta.francia@polito.it (C.F.)

* Author to whom correspondence should be addressed; E-Mail: stefania.specchia@polito.it; Tel.: +39-011-090-4608; Fax: +39-011-090-4624.

Abstract: Platinum (Pt) nanoparticles are deposited on a hybrid support (C-MnO₂) according to a polyol method. The home-made catalyst, resulted as Pt/C-Mn$_x$O$_{1+x}$, is compared with two different commercial platinum based materials (Pt/C and PtRu/C). The synthesized catalyst is characterized by means of FESEM, XRD, ICP-MS, XPS and μRS analyses. MnO₂ is synthesized and deposited over a commercial grade of carbon (Vulcan XC72) by facile reduction of potassium permanganate in acidic solution. Pt nanoparticles are synthesized on the hybrid support by a polyol thermal assisted method (microwave irradiation), followed by an annealing at 600 °C. The obtained catalyst displays a support constituted by a mixture of manganese oxides (Mn₂O₃ and Mn₃O₄) with a Pt loading of 19 wt. %. The electro-catalytic activity towards MOR is assessed by RDE in acid conditions (0.5 M H₂SO₄), evaluating the ability to oxidize methanol in 1 M concentration. The synthesized Pt/C-Mn$_x$O$_{1+x}$ catalyst shows good activity as well as good stability compared to the commercial Pt/C based catalyst.

Keywords: rotating disk electrode; platinum nanoparticles; hybrid support; manganese oxides; methanol oxidation reaction (MOR); CO stripping

1. Introduction

Fuel cells are electrochemical devices that produce electricity from the energy of a fuel through a highly efficient conversion process, resulting in low emissions and low environmental impact [1]. Between the different types of fuel cell, Direct Alcohol Fuel Cells (DAFC) and more specifically, Direct Methanol Fuel Cells (DMFC), represent a valid alternative for small portable electronic devices and auxiliary power units, due to the high energy density of alcohols, their lightweight and compact nature and their ability for fast recharging [2,3].

Platinum is the most widely used catalyst for both the anodic methanol oxidation reaction (MOR) and the cathodic oxygen reduction reaction (ORR) [4,5]. Pt is considered the most suitable electro-catalyst for MOR due to its high activity and stability, especially in acidic media [6]. However, one of the main barriers to the commercialization of DMFC technologies is still the high cost of Pt. To reduce the cost, an improvement of the performance of conventional Pt-based catalysts is necessary. This would lead to a reduction of the total Pt loading on the electrode. For this purpose, reaction rates need to be enhanced (*i.e.*, the overvoltage needs to be decreased) by modifying the catalyst composition or structure, to produce a more active electro-catalytic material [7].

A common approach to enhance the activity of Pt involves well dispersed nanoparticle structures, avoiding agglomeration and increasing utilization [7]. Further optimization of Pt-based electro-catalysts has been achieved through the formation of bi-metallic alloys such as PtCo and PtNi (for cathodic ORR) and PtRu (for anodic MOR) [8,9]. It has also been demonstrated that efficiency can be further improved by promotion of methanol electro-oxidation by means of various metal oxides-, carbides- and nitrides-promoted electro-catalysts. Non-noble metal oxides (M-O$_x$) such as WO$_3$, CeO$_2$, V$_2$O$_5$, Nb$_2$O$_5$, MoO$_x$, ZrO$_2$, TiO$_2$, MgO and MnO$_2$, exhibit suitable surface properties which can efficiently promote the methanol and ethanol electro-oxidation reactions combined with Pt/C [10]. Therefore, a good strategy to improve the catalytic activity of Pt-based catalysts for MOR is to use metal oxides in the catalyst supports, as a hybrid structure (C + M-O$_x$) [11]. Pure Pt, in fact, is readily poisoned by strongly-adsorbed intermediates, of which CO is consistently considered as one of the main poisoning species at low operating temperature [12].

The use of metal oxide-containing Pt/C electro-catalysts has been reported to effectively enhance the electro-oxidation of methanol by the spillover of CO on Pt sites to the adjacent metal oxides. These oxides are supposedly capable of adsorbing large quantities of –OH species, which are then donated to the neighboring Pt sites where stepwise methanol dehydrogenation occurs. Metal oxides also provide suitable functional groups which strongly interact with small Pt crystallites, impeding their random growth and agglomeration during device operation for longer duration. In particular, high surface area metal oxides used as supports or matrices, are capable of physically separating metal particles (to diminish their tendency to undergo degradation by agglomeration) and of interacting mutually with them, thus affecting their chemisorptive and catalytic properties. Oxides are often thought as insulating or semi-conducting materials but certain non-stoichiometric oxides existing in various valance states exhibit conductivity not much lower than that of metals and possess appreciable catalytic activity [7]. In electro-catalysis, the reactions occur at the interface, so surface reactivity is very important. Redox reactions of metal oxides involve both ion and electron transfer processes. The electron transfer reactions are influenced by the distribution of electronic states in the electrolyte

and within the oxide. When oxides are in contact with aqueous solutions, their surfaces are covered with –OH groups; their actual population depends on the nature of the oxide and its specific crystal face. Some metal oxides are more hydrous than the others. The hydrous behavior, which varies from oxide to oxide, favors proton mobility and affects overall reactivity [7].

MnO_2 has been used in a wide range of applications such as catalyst, molecular-sieves, ion-sieves, batteries and magnetic materials due to its excellent physicochemical properties [13]. Manganese oxides were widely used as catalyst support for fuel cells due to their promoting effects in the oxidation of small organic molecules, such as the excellent proton conductivity, the increase of catalyst utilization and the synergistic effect between catalysts and manganese oxides [6]. In particular, MnO_2 possesses good proton-electron intercalation properties and is known to show good electro-chemical properties under various operating conditions [10]. Mn possesses a wide range of oxidation states and such oxo-manganese species are generally strong chemical oxidants. Due to the possibility of the Mn^{4+}/Mn^{3+} redox couple and the presence of labile oxygen, MnO_2 shows high promoting and anti-poisoning activities for alcohol electro-oxidation [7]. The main reasons for effectiveness of MnO_2 as a promoter are attributed to its surface area, tunnel structure and crystal phase. It is known that oxides with one-dimensional structures such as nanorods, nanowires and nanotubes possess distinctive crystalline phase states, as compared to their bulk counterparts [10]. It is also known that the interaction between metal crystallites and an oxide surface is influenced by the nature of interfacial contact and the crystalline characteristic of the oxide. MnO_2 with smaller and uniform crystalline orientation as well as suitable surface morphology should offer apposite active sites for facile interaction with Pt crystallites, which can provide optimized synergistic effect for alcohol electro-oxidation [14]. However, the effect of microstructure/morphology of manganese oxides on the nature of Pt dispersion on Mn_xO_{1+x}/carbon-based electrocatalysts has not been extensively investigated so far [10].

In this work, α-MnO_2 was synthesized and deposited on a commercial carbon black (Vulcan XC-72). Then, Pt nanoparticles were deposited on the formed hybrid support (C-MnO_2), called Pt/C-Mn_xO_{1+x}, by a microwave-assisted polyol method followed by a thermal treatment in inert atmosphere at 600 °C. The synthesized catalyst was compared with two commercial Pt-based catalysts characterized and tested for MOR in acidic medium.

2. Results and Discussion

2.1. Physical-Chemical Characterization

The XRD pattern of the prepared C-MnO_2 is given in Figure 1A. The broad peak at about 23.5° is attributed to the graphitic carbon support. All other peaks are clearly indexed to the pure tetragonal phase of α-MnO_2 (JCPDS card #44-0141), with lattice constants of a = 9.73 Å and c = 2.84 Å. No peaks were observed for other types of crystals or amorphous MnO_2 which confirmed the purity of the prepared sample. The intensive diffraction peaks appeared at 12.46°, 18.08°, 28.83°, 37.00°, 37.66°, 41.95°, 50.13°, 60.36°, 66.30°, 72.87°, respectively, which are characteristic peaks of α-MnO_2 with the major peaks intensity at 18.08° [15,16]. α-MnO_2 is constructed from the double chains of edge-sharing MnO_6 octahedra, which are linked at the corners to form tunnel structures [17].
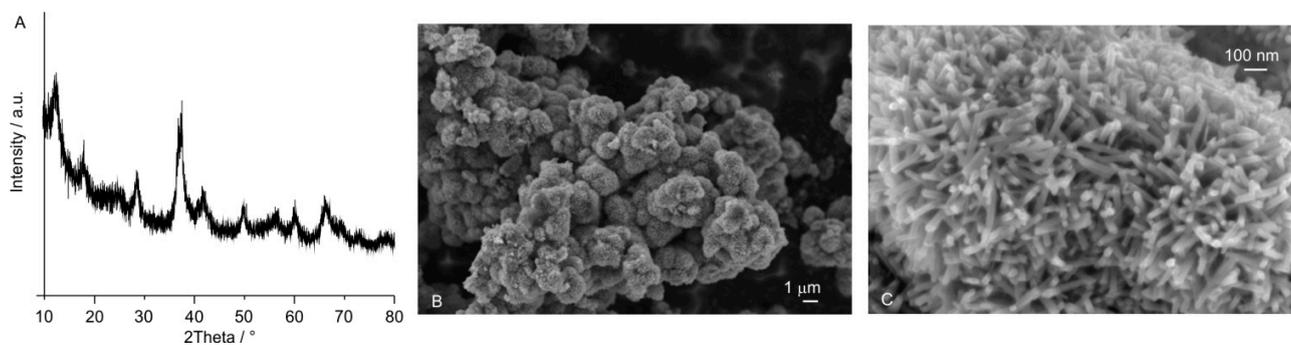
Figure 1. C-MnO$_2$ support: (**A**) XRD patterns; (**B**,**C**) FESEM images at different magnification.

The morphology of prepared C-MnO$_2$ was investigated by FESEM and the corresponding micrographs are shown in Figure 1B,C. MnO$_2$ nanocrystals grow up on the carbon black, forming sphere-like micro-particles with an average diameter of about 1 μm (Figure 1B). At higher magnification (Figure 1C), the outside part of the particles appeared to be urchins, homogeneously composed of densely aligned nanorods with uniform diameter of about 35 nm. The percentage of MnO$_2$ in the hybrid support evaluated by ICP-MS technique is 64.8 wt. %. This value is very close to the theoretical wt. % percentage of MnO$_2$ expected for the adopted synthesis, which is equal to 68.4 wt. %. Thus, the synthesis method adopted allows a very precise control of the mass loading level of nanostructured MnO$_2$ onto the carbon material by controlling the ratio between KMnO$_4$ and Vulcan XC-72 carbon.

XRD patterns were acquired for all catalysts supported on carbon (Figure 2). X-ray spectra exhibited the characteristic peaks corresponding to the Pt face-centered cubic (*fcc*) polycrystalline structure (111, 200, 220 and 311 reflection planes), consistent with the XRD pattern of JCPDS card #00-4-0802 (2θ = 39.76°, 46.24°, 67.45°, 81.28°). A signal near to 25° (2θ) was obtained, which corresponds to the (002) graphite basal planes for Pt/C and PtRu/C [18]. This peak is not appreciable on Pt/C-Mn$_x$O$_{1+x}$ because of the high manganese oxides content. No metallic Ru diffraction peaks were detected in the commercial PtRu/C which is an indication of alloyed PtRu as reported in the literature [19]. As can be seen in Figure 2, Pt diffraction peaks of the commercial PtRu/C shifted to a positive 2θ value compared with that of Pt/C which reveals alloy formation. Formation of solid solution between Pt and Ru by replacing of Pt with smaller Ru atoms in the lattice points of Pt *fcc* structure results in the reduction of lattice parameter and positive shift of *fcc* diffraction signals [20,21]. It is well known that the alloying of Pt with Ru leads to a decrease in the interatomic bond length because of the smaller Ru atomic radius [22].

Particle diameters were calculated by the Debye-Scherrer equation for all catalyst used. 1.7, 4.5 and 4 nm were obtained for Pt/C-Mn$_x$O$_{1+x}$, Pt/C and PtRu/C, respectively, with lattice parameter of 3.78, 3.93 and 3.82 Å, respectively. According to ICP-MS analysis, the Pt wt. % loading for the three Pt/C-Mn$_x$O$_{1+x}$, Pt/C and PtRu/C was equal to 19, 20 and 38 wt. %, respectively.
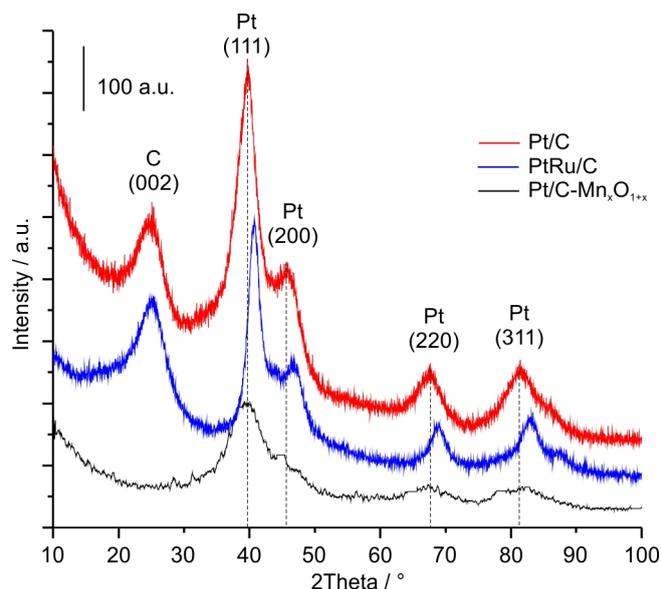
Figure 2. XRD patterns of Pt/C, PtRu/C and Pt/C-Mn$_x$O$_{1+x}$, with the characteristic Miller indexes of Pt *fcc* (JCPSD card #00-4-0802).

The Mn 2p XPS spectrum in Figure 3A exhibited Mn 2p$_{1/2}$ at 653.52 eV and Mn 2p$_{3/2}$ at 641.71 eV, in which the spin-energy separation of 11.79 eV which indicates that the element manganese in the sample exists in the chemical state of Mn^{2+} and Mn^{4+} and therefore the formation of MnO$_2$, Mn$_2$O$_3$ and Mn$_3$O$_4$ [23–25]. As shown in Figure 3B, the Pt 4f spectrum of the Pt/C-Mn$_x$O$_{1+x}$ was deconvoluted into two doublet peaks, corresponding to a spin-orbit splitting of 4f$_{7/2}$ and 4f$_{5/2}$ states of ca. 3.33 eV. The most intense doublet at 71.45 (4f$_{7/2}$) and 74.78 eV (4f$_{5/2}$) was due to the metallic Pt, corresponding to metallic platinum particles (Pt^0) [4,6,10,13,17].
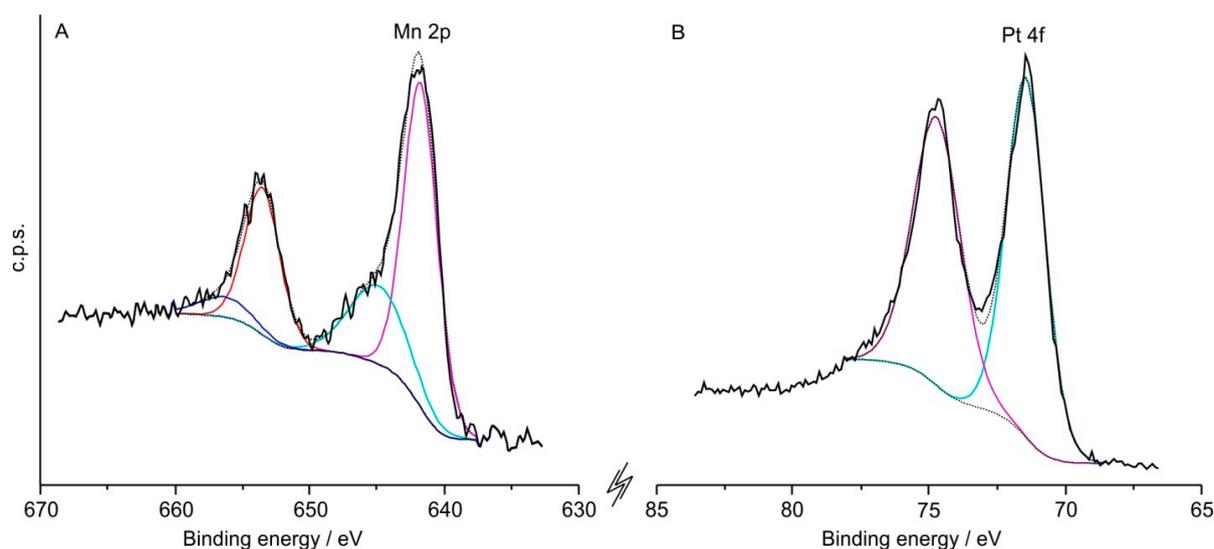
Figure 3. XPS deconvolution of Pt/C-Mn$_x$O$_{1+x}$: (**A**) high resolution Mn 2p spectrum; (**B**) high resolution Pt 4f spectrum.

To assess the chemical structure of the Pt/C-Mn$_x$O$_{1+x}$ catalyst, an extra sample of MnO$_2$ annealed at 600 °C (same temperature used to anchor Pt nanoparticles on the C-MnO$_2$ support) was examined by μRS. Raman spectra in different points of the annealed oxide (Figure 4) show the presence of two

types of oxides structure, the Mn_3O_4 hausmannite spinel-like and the Mn_2O_3 bixbyite. Specifically, five characteristic Raman peaks for the spinel structure [$\nu1 = 310$ cm^{-1}, $\nu2 = 357$ cm^{-1}, $\nu3 = 485$ cm^{-1}, $\nu4 = 579$ cm^{-1}, $\nu5 = 653$ cm^{-1}] and for the bixbyite [$\nu1 = 263$ cm^{-1}, $\nu2 = 308$ cm^{-1}, $\nu3 = 512$ cm^{-1}, $\nu4 = 631$ cm^{-1}, $\nu5 = 670$ cm^{-1}] were detected, suggesting the presence of a mix of oxides [26]. In fact, according to the literature [27–29], in inert atmosphere at around 500 °C MnO_2 is reduced to Mn_2O_3 and further reduced to Mn_3O_4 at 900 °C. These results are in line with the presence of the mixture of hausmannite and bixbyite manganese oxides on the final Pt/C-Mn_xO_{1+x} catalyst, annealed at 600 °C in nitrogen atmosphere, as pointed out by XPS analysis.
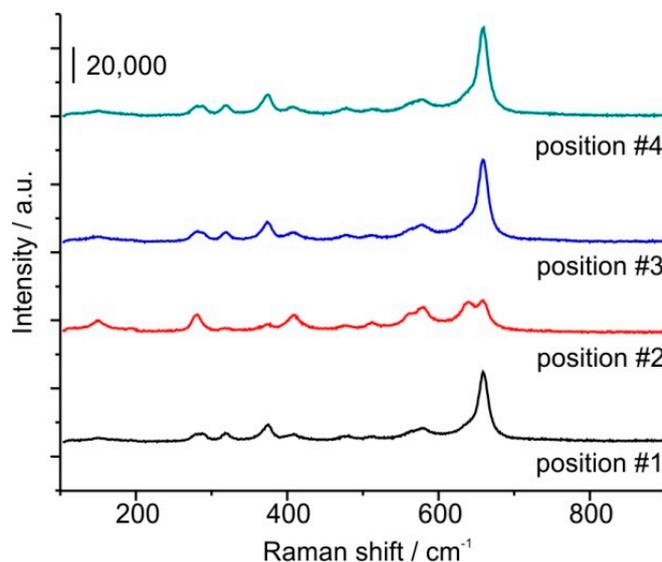

Figure 4. Raman spectra ($\lambda = 785$ nm) of MnO_2 annealed at 600 °C in four different areas of the examined sample (denoted as position #1–#4).

2.2. Electro-Chemical Characterization

The CV profiles recorded in N_2-saturated 0.5 M H_2SO_4 (Figure 5) exhibit defined regions of hydrogen underpotential, adsorption/desorption and platinum oxide formation/reduction for all the samples. In particular, the hydrogen adsorption/desorption peaks shapes are similar for the Pt/C-Mn_xO_{1+x} and the commercial Pt/C, with the latter exhibiting a higher hydrogen desorption area. The electrochemical active surface area (ECSA) resulted 44.1 m$^2 \cdot$g^{-1} for Pt/C-Mn_xO_{1+x} and 45.4 m$^2 \cdot$g^{-1} for Pt/C, respectively. For the PtRu/C catalyst the peak shape is different from the previous ones, with a sharper hydrogen desorption peak typical for the PtRu based catalysts [30,31] and ECSA of 69.8 m$^2 \cdot$g^{-1}. Regarding the Pt oxides reduction peak, for the Pt/C-Mn_xO_{1+x} it is shifted towards more positive potentials of about 100 mV in comparison with the commercial Pt/C catalyst. This could indicate a lower oxygen reduction overpotential if this catalyst should be used as a cathode catalyst for a PEMFC [32]. Otherwise, for the PtRu/C catalyst, the same peak is about 200 mV shifted to more negative potentials. This is also typical for PtRu based catalysts [21]. The similar ECSA values for the Pt/C-Mn_xO_{1+x} and Pt/C catalysts could be due to the similar Pt content of these catalysts, equal to 19 wt. % and 20 wt. %, respectively, according to ICP-MS analysis, whereas the measured Pt content of PtRu/C was almost double compared to the other two catalysts. Moreover, the presence of a

high amount of manganese oxides on the surface of Pt/C-Mn$_x$O$_{1+x}$ (see previous discussion on XPS and μRS) could result in a low electrical conductivity of the electrode [13,33,34].
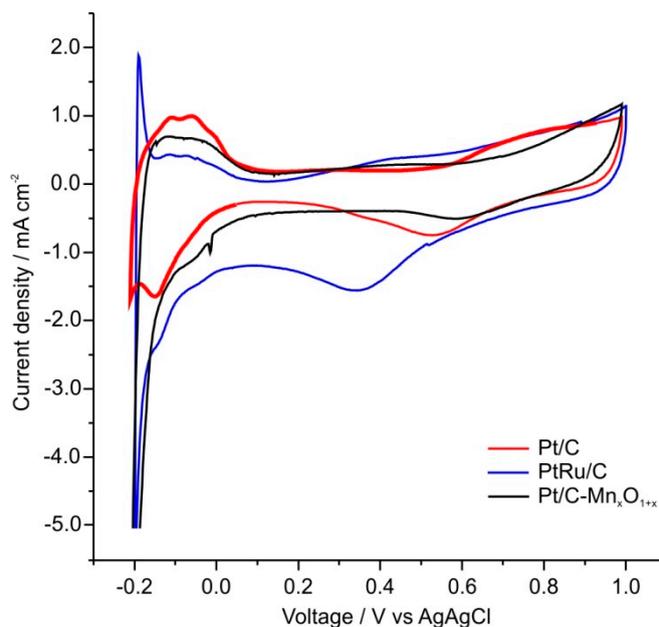
Figure 5. CV of Pt/C, PtRu/C and Pt/C-Mn$_x$O$_{1+x}$ recorded at 10 mV·s^{-1} (N$_2$-saturated in 0.5 M H$_2$SO$_4$, 0.1 ITC mass ratio, 20 mg$_{Pt}$·cm^{-2} catalyst loading).

CO stripping voltammetries are shown in Figure 6. The first cycle of the CO stripping voltammetry profile of each one of the three samples shows the CO electro-oxidation peak. Then, in the second cycle, only typical hydrogen underpotential deposition and Pt oxides formation/reduction phenomena are evident. This essentially shows the complete oxidation of adsorbed CO during the first voltammetry scan leaving the active Pt surface clean [10,13,35,36].
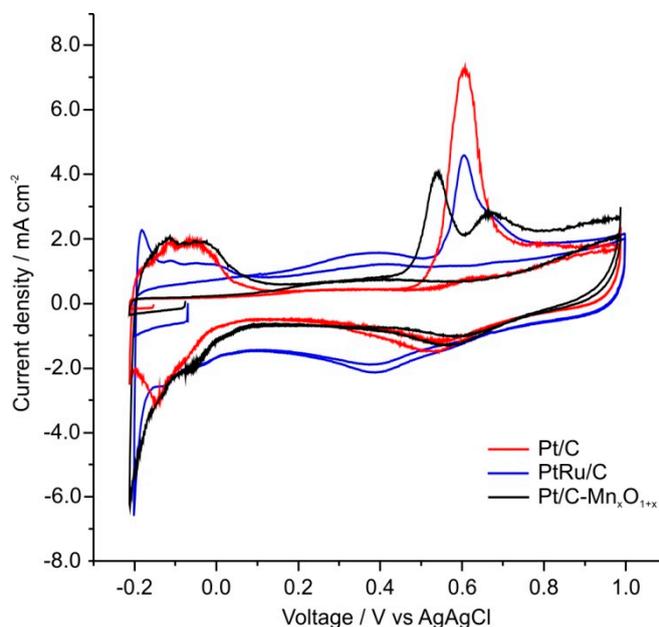
Figure 6. CO stripping voltammetries of Pt/C, PtRu/C and Pt/C-Mn$_x$O$_{1+x}$ recorded at 20 mV·s^{-1} (0.5 M H$_2$SO$_4$, 0.1 ITC mass ratio, 20 mg$_{Pt}$·cm^{-2} catalyst loading).
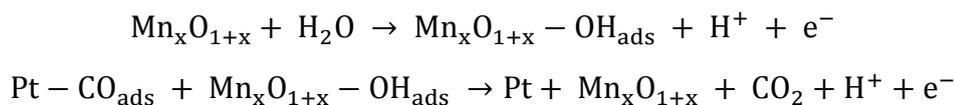
The onset potential of CO electro-oxidation, taken as the potential at which 5% of the maximum current was reached, was of 0.61, 0.59 and 0.54 V for the commercial Pt/C, the PtRu/C and the Pt/C-Mn_xO_{1+x} catalysts, respectively (see Table 1). A negative shift of this onset potential indicates an enhanced catalytic activity for CO oxidation. This has been extensively reported for PtRu catalysts [18,20,21]. In the case of Pt-transition metal oxide based catalysts this effect can also be observed [14]. In particular, for our Pt/C-Mn_xO_{1+x} catalyst, the onset potential is 70 mV lower than for the commercial Pt/C catalyst.

Table 1. CO stripping potential, MOR peak potential of the forward scan and I_f/I_b ratio in the CV curves of Pt/C-Mn_xO_{1+x}, Pt/C and Pt-Ru/C in 0.5 M H_2SO_4 and 1 M MeOH.

| Catalysts	CO Stripping Peak Position V *vs.* Ag/AgCl	MOR forward Peak Position V *vs.* Ag/AgCl	MOR I_f/I_b
Pt/C-Mn_xO_{1+x}	0.54	0.66	1.54
Pt/C	0.61	0.80	0.92
PtRu/C	0.59	0.66	1.92

Analyzing more in detail the CO stripping peak's shape, it can be observed that the commercial Pt/C peak has a symmetric shape, while the Pt/C-Mn_xO_{1+x} catalyst exhibits a second lower and broader peak at higher potentials than the main peak. The presence of the double peak could be due to the presence of both Pt predominant crystal face or Pt agglomerates [37,38]. In fact, the oxidation of a monolayer of CO is strongly influenced by the particle size of Pt. Pt agglomerates show a notable activity towards CO oxidation compared to isolated Pt particles. Moreover, the presence of the double peak for Pt/MnO_2/C hybrid catalysts has been noticed by other authors as well [10,39]. In fact, the CO stripping from the Pt surface in the presence of MnO_2 occurs via a kind of synergic effect between the OH_{ads} on MnO_2 and the CO_{ads} on Pt [10]. The double peak due to CO stripping from the Pt/C-Mn_xO_{1+x} could be linked with the possible formation of labile OH species on the triple-phase interface between the Pt, the oxide and the electrolyte, which provides electronic suitability for the oxidation of CO species on the Pt surface [39]. It has been demonstrated that MnO_2 nanorods promoted Pt/C catalysts showed larger negative shift in the CO electro-oxidation peak potential due to OH_{ads} species on the MnO_2 that tend to electronically weaken the Pt-CO bond and promote the oxidation of CO to CO_2 [10]. The presence of MnO_2 in a MnO_2-Pt/C composite electrode primarily plays a catalytic role in the ORR. It enhances the catalytic behavior of Pt for the ORR by substituting for oxygen as an electron-acceptor in the case of oxygen starvation [40]. Furthermore, based on studies on Pt/Mn_3O_4-MWCNT [33], the Mn_3O_4 leads to uniform and small Pt nanoparticle deposition, with enhanced CO-tolerance and excellent stability in methanol oxidation. In fact, Mn_3O_4 nanoparticles promote the dissociation of coordinated water and further oxidize CO_{ads} to release more Pt active sites [33]. The hydrous Mn_3O_4 would use its inherent Mn_3O_4–OH bonds to directly donate the hydroxide species to the Pt sites and oxidize the adsorbed CO species [41]. Mn_3O_4 is also known for favoring the growth of Pt nanoparticles with high index facets [33,42]. Consequently, in our Pt/C-Mn_xO_{1+x} catalyst, where a mix of manganese oxides is present, both mechanisms could be involved. The promotional CO stripping from the Pt surface in the presence of manganese oxides

occurs via a type of synergic effect as reported in the literature [10,39]. Overall, the following reaction mechanism can be assumed:

$$Mn_xO_{1+x} + H_2O \rightarrow Mn_xO_{1+x} - OH_{ads} + H^+ + e^-$$

$$Pt - CO_{ads} + Mn_xO_{1+x} - OH_{ads} \rightarrow Pt + Mn_xO_{1+x} + CO_2 + H^+ + e^-$$

The PtRu/C catalyst peak appears to be more asymmetric, with a broadening towards higher overpotentials. Thus, the presence of MnO_2 on the surface of the carbon support causes a co-catalytic action which promotes the CO oxidation catalytic effect of Pt.

The electro-catalytic activity toward MOR of the three catalysts was investigated by cyclic voltammetry using a 0.5 M H_2SO_4 and 1.0 M MeOH solution as electrolyte (Figure 7). For all of the catalysts, the voltammograms exhibit two characteristics oxidation peaks. The first peak is observed during the anodic potential sweep and it is characteristic of the oxidation of methanol adsorbed on the Pt surface. This oxidation occurs in multiple steps, with the production of carboxyl intermediates and strongly adsorbed CO species, as discussed in the literature [43]. Mainly formic acid and formaldehyde have been found during methanol oxidation on Pt surface, as intermediate products [44]. With the potential increase, after the forward peak, the oxidation current decreases, due to the poisoning effect of the CO species strongly adsorbed on Pt and to the Pt oxides formation, which passivates the Pt surface [45]. The second peak appears during the cathodic potential sweep (reverse scan) and it is attributed to the oxidation of adsorbed CO species and/or to the oxidation of further methanol on the Pt oxide surface formed during the anodic scan [10]. During electro-oxidation of MeOH, strongly adsorbed carbonaceous species inhibit further adsorption of MeOH on the catalyst surface, which causes a positive shift in the onset potential and a decrease in the current at a specific potential. Therefore, the more the forward scan peak is shifted to negative potentials, the greater the promotion effect of the electro-catalyst [18].
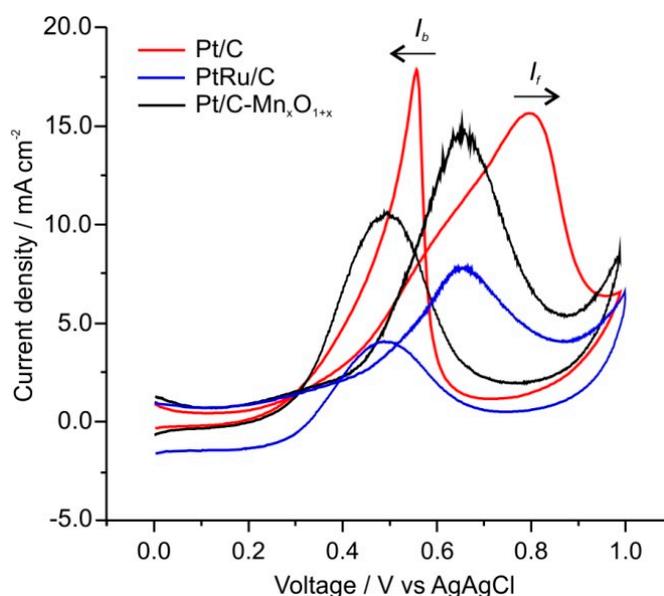
Figure 7. CV of Pt/C, PtRu/C and Pt/C-Mn$_x$O$_{1+x}$ towards MOR 1 M MeOH recorded at 20 mV·s^{-1} (0.5 M H_2SO_4, 1 M MeOH, 0.1 ITC mass ratio, 20 mg$_{Pt}$·cm^{-2} catalyst loading).

The forward peak potentials for the Pt/C-Mn$_x$O$_{1+x}$, Pt/C and PtRu/C catalysts obtained from the CV are shown in Table 1. The value of the ratio between the forward peak maximum current density (I_f) and the backward peak maximum current density (I_b) is also shown in Table 1. The higher this I_f/I_b ratio is, the greater the electro-catalyst's resistance to poisoning is [46]. Hence, the value of I_f/I_b can be viewed as an index of the tolerance of a catalyst to poisoning species, *i.e.*, adsorbed CO molecules. From these results, it can be concluded that the Pt/C-Mn$_x$O$_{1+x}$ catalyst is a stronger promoter than the commercial Pt/C catalyst for the MOR and this is in agreement with the CO stripping results. In much of the literature, adsorbed CO is considered as a poisoning intermediate for MOR on pure Pt surface. To remove CO from the Pt surface, adsorbed OH species generated from water activation are indispensable. However, a high potential is needed to activate water on the Pt surface. In PtRu catalysts, water activation can occur at lower potential on Ru-sites. Therefore, MOR activity on PtRu catalysts can be enhanced through the bi-functional mechanism [44].

The durability of the electrodes was measured via an accelerated durability test (ADT) at room temperature up to 5000 consecutive cycles for the Pt/C-Mn$_x$O$_{1+x}$ catalyst and up to 4000 cycles for the Pt/C one. A noticeable corrosion of carbon nanostructures as Pt supports, confirmed from the reduction of the catalyst thickness from oxidation of carbon, agglomeration and detaching of Pt, had already been reported by other researcher groups, as well [23]. Figure 8 compares voltammograms before and after stability tests. The results show that Pt/C-Mn$_x$O$_{1+x}$ is more stable compared to Pt/C, showing an increase of ECSA (+29% after 5000 cycles, Figure 8A). In fact, its CV increased progressively up to 1000 cycles, remaining then stable up to the end of the ADT at 5000 cycles. On the contrary, the Pt/C lost continuously stability cycle after cycle, with an overall decrease of ECSA equal to −9% after 4000 cycles (Figure 8B). According to the literature [47], the ECSA increase of Pt/C-Mn$_x$O$_{1+x}$ could be due to a re-arrangement of Pt over carbon. This re-arrangement is not a stable condition, but a reversible process. In fact, as observed for Pt/C-Mn$_x$O$_{1+x}$ during CO stripping analysis (Figure 6), Pt nanoparticles agglomeration can evolve to more disperse Pt nanoparticles or different Pt nano-shape islands depending on the stress cycling adopted for accelerated degradation procedure [47,48].
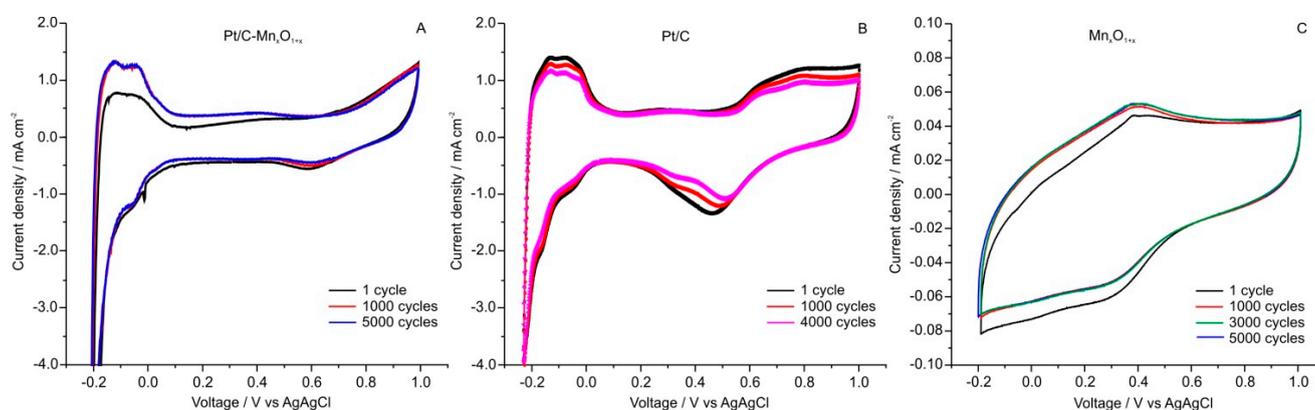
Figure 8. CV after consecutive potential cycling recorded at 50 mV·s^{-1}: (**A**) Pt/C-Mn$_x$O$_{1+x}$; (**B**) Pt/C; (**C**) Mn$_x$O$_{1+x}$ (0.5 M H$_2$SO$_4$, 0.1 ITC mass ratio, 20 mg$_{Pt}$·cm^{-2} catalyst loading).

To better check stability of the Pt/C-Mn$_x$O$_{1+x}$ and in particular of the Mn$_x$O$_{1+x}$ support, the extra Mn$_x$O$_{1+x}$ sample used for µRS analysis (Figure 4) was used to assess its stability in acid conditions. Specifically an RDE prepared with pure Mn$_x$O$_{1+x}$, was subjected to ADT by cycling it 5000 times in

the same conditions used for the Pt/C-Mn$_x$O$_{1+x}$ (50 mV·s^{-1} between 0.4 and 0.8 V *vs.* Ag/AgCl, in a 0.5 M H$_2$SO$_4$ solution). Results from CV degradation (Figure 8C) show very little degradation, sign that Mn$_x$O$_{1+x}$ is a stable support in acid environment, as reported in the literature as well [29,40,48,49]. Moreover, this RDE was analyzed directly by SEM coupled with EDX detector before and after ADT. Images of this RDE are shown in Figure S1 of the supporting info. From a visual point of view, the Mn$_x$O$_{1+x}$ on RDE after cycling showed a rearrangement compared to the fresh configuration: it appears more agglomerated near the edges of the disk (Figure S1C,D), whether in the fresh configuration the electrode appears more homogeneous (Figure S1A,B). EDX elementary analyses on the overall Mn atomic quantity available on the RDE before and after ADT enlightened that after cycling the Mn overall content diminished by 18%. Thus, Mn$_x$O$_{1+x}$, can be considered a stable support in acidic environment. The presence of manganese oxides in a Pt/C composite electrode plays a catalytic role in the ORR by enhancing the catalytic behavior of Pt for the ORR [40]. In fact, manganese oxides in the composite electrode can be considered as substitute for oxygen as an electron-acceptor in the case of oxygen starvation.

3. Experimental Section

3.1. Chemicals

Vulcan XC-72 was purchased from Cabot. Chloroplatinic acid hexahydrate (H$_2$PtCl$_6$·6H$_2$O) $\geq$ 37.50% Pt basis, potassium permanganate (KMnO$_4$), potassium hydroxide 85 wt. % (KOH), ethylene glycol 98 wt. % (EG, HOCH$_2$CH$_2$OH), isopropyl alcohol 99.7 wt. % ((CH$_3$)$_2$CHOH), sulfuric acid (H$_2$SO$_4$) 98 wt. %, Nafion$^{®}$ perfuorinated resin 5 wt. % hydro-alcoholic solution and methanol (MeOH, CH$_3$OH) 99.8 wt. % were purchased from Sigma Aldrich Italia (Milano, Italy). Commercial 20 wt. % Pt/Vulcan XC-72 electrocatalyst (QuinTech QuinTech e.K., Göppingen, Germany) and commercial PtRu
1:1 at % (Hispec 6000, Alfa Aesar GmbH & Co KG, Karlsruhe, Germany) were used for comparison tests. Nitrogen (99.999% purity) and diluted carbon monoxide (10 vol % CO in Ar) gases were supplied in cylinders by SIAD S.p.A. (Bergamo, Italy). All aqueous solutions were prepared using ultrapure water obtained from a Millipore Milli-Q system (Merck KGaA, Darmstadt, Germany) with resistivity > 18 mΩ·cm^{-1}.

3.2. Synthesis of the Hybrid Support C-MnO$_2$

To prepare the C-MnO$_2$, 3.9 g of KMnO$_4$ and 12.6 g of H$_2$SO$_4$ were added into 130 g of deionized water under magnetic stirring to form the precursor solution. Then, 1.0 g of Vulcan XC-72 was added into this precursor solution. Subsequently, the formed suspension was heated up to 80 °C and kept at 80 °C for 6 h under magnetic stirring. The precipitates were filtered and washed with distilled water. Finally, the obtained powder was dried at 120 °C for 6 h under vacuum. Assuming that all the KMnO$_4$ used in the synthesis can be reduced to MnO$_2$, the theoretical wt. % of MnO$_2$ in the C-MnO$_2$ support is equal to 68.4 wt. %.

3.3. Synthesis of the Pt/C-Mn$_x$O$_{1+x}$ Catalyst by Thermal Method

For the synthesis of Pt/C-Mn$_x$O$_{1+x}$ catalyst, 200 mg of the previously prepared C-MnO$_2$ was added to 50 mL EG and the mixture was stirred for 30 min. Then, H$_2$PtCl$_6$·6H$_2$O was dissolved into the EG solution under stirring. The pH was adjusted to 12, by the addition of 1 M KOH in EG solution. Microwave irradiation was applied to the solution at 700 W for 2 min, in order to reduce the Pt^{4+} ions to metallic Pt^0. The solution was left to cool naturally to room temperature. After cooling, some drops of acetone were added to the solution and the Pt/C-Mn$_x$O$_{1+x}$ catalyst was washed thoroughly with abundant water. Finally, the catalyst was annealed under nitrogen atmosphere for 2 h at 600 °C.

3.4. Synthesis of the PtRu/C Catalyst

PtRu/C catalyst was prepared by adding 60 wt. % [50] commercial PtRu 1:1 at % on functionalized Vulcan XC72 into a water-isopropyl alcohol solution under stirring for 24 h. Then the PtRu/C catalyst was centrifuged and dried.

3.5. Chemical-Physical Characterization

Field-emission scanning electron microscopy (FESEM JEOL-JSM-6700F instrument, FEI Europe, Eindhoven, The Netherlands) coupled with an Energy Dispersive X-ray Spectrometry Detector (EDX OXFORD INCA, EDAX Inc., Mahwah, NJ, U.S.A.) and scanning electron microscopy (SEM-EXD FEI-QuantaTM Inspect 200, FEI Europe, Eindhoven, The Netherlands, with EDAX PV 9900 instrument, working at 15 kV, EDAX Inc., Mahwah, NJ, USA) were performed to analyze the morphology and check the amount of Pt and Mn.

The MnO$_2$ and platinum-to-carbon weight percentage in the catalysts was determined by inductively coupled plasma atomic mass spectroscopy (ICP-MS ICAP-Q instrument, ThermoFisher Scientific Inc., Waltham, MA, USA). Prior to analysis, the samples were digested in hot concentrated HCl/HNO$_3$ 3:1 mixture with some droplets of H$_2$SO$_4$.

The XRD reflections were recorded on a PANalytical X'Pert PRO diffractomer with a PIXcel detector (PANalytical B.V., Almelo, The Netherlands), using Cu Kα radiation, under the conditions of $2\theta = 10°–100°$ and 2θ step size = 0.03, in order to examine the different polymorphs.

X-ray photoelectron spectroscopy (XPS) was performed to determine the elemental surface composition of the catalysts. The analysis was carried out using a Physical Electronics PHI 5000 Versa Probe electron spectrometer system (Physical Electronics Inc., Chanhassen, MN, USA) with monochromated Al Kα X-ray source (1486.60 eV) run at 15 kV and 1 mA anode current. The survey spectra were collected from 0 to 1200 eV. The narrow Mn 2p spectra were collected from 635 to 665 eV, the narrow Pt 4f spectra from 66 to 86 eV and the narrow C 1s spectra from 280 to 293 eV. All of the spectra were calibrated against a value of the C 1s binding energy of 284.5 eV. Multipak 9.0 software (Physical Electronics Inc., Chanhassen, MN, USA) was used for obtaining semi-quantitative atomic percentage compositions, using Gauss-Lorentz equations with Shirley-type background. A Gaussian/Lorentzian 70%/30% line shape was used to evaluate peak positions and areas of the high resolution Pt 4f and Mn 2p spectra, with a standard deviation in locating the peaks equal to 0.3 eV.

The chemical structure of the support was analyzed by a μ-Raman Spectroscopy (μRS Renishaw InVia spectrometer equipped with a Leica DMLM confocal microscope and a CCD detector with an excitation wavelength of 785 nm, Renishaw plc, Gloucestershire, United Kingdom). The Raman scattered light was collected in the spectral range 100–1000 cm^{-1}. At least ten scans were accumulated in four different positions of the catalyst to ensure a sufficient signal to noise ratio.

3.6. Electro-Chemical Characterization

The prepared electro-catalysts were tested in a conventional three-compartment electrochemical cell using a multi-potentiostat (Bio-Logic SP150, Bio-Logic Science Instruments SAS, Claix, France) and a rotating ring-disk electrode instrument (RRDE-3A ALS Model 2323, ALS Co. Ltd, Tokyo, Japan). The electrolyte was 0.5 M H_2SO_4 aqueous solution saturated with either N_2 or CO 10% *v/v* in Ar by direct bubbling the gas into the solution. For RDE measurements, the cell was equipped with a glassy carbon (GC) disk working electrode (0.1256 cm^2 geometric area), a Pt helical wire counter electrode and a silver chloride electrode (Ag/AgCl) as reference electrode. Glassy carbon (GC) electrodes were polished with alumina powder, ultrasonic washing and blow drying, before dropping the catalyst ink. Different GC disk electrodes were arranged by preparing the ink using an ionomer-to-catalyst (ITC) mass ratio (mg of Nafion® over mg of catalyst) equal to 0.1 and catalyst loading of 20 μg$_{Pt}$·cm^{-2} [51]. The working electrode was surface-polished with 1 and 0.06 μm alumina powders to a mirror-like finish its surface and sonicated to remove alumina particles before each experiment. Cyclic voltammograms (CV) with either N_2 or CO 10 vol % in Ar were recorded at 10 mV·s^{-1} and 20 mV·s^{-1}, respectively.

CO stripping voltammetry was performed in 0.5 M H_2SO_4 at a scan rate of 20 mV·s^{-1}. Prior to analysis a flow rate of 10 vol % CO in Ar was pre-adsorbed for 30 min while maintaining the working electrode at the constant potential of −0.19 V (*vs.* Ag/AgCl) and rotating disk speed of 900 rpm. Afterwards, a flow rate of pure N_2 was used for 15 min to remove the CO reversibly adsorbed onto the surface and the excess CO dissolved in the solution.

Cyclic voltammetries for the methanol oxidation reaction in acid conditions were carried out in a 0.5 M H_2SO_4 solution with 1 M MeOH. The scan rate was 20 mV·s^{-1} and the potential window was 0.0–1.0 V *vs.* Ag/AgCl. The highest initial activity was usually obtained within ~20 cycles and then the experiment was stopped [52].

The electrocatalyst stability was performed by ADT cycling up catalysts to 5000 times between 0.4 and 0.8 V *vs.* Ag/AgCl forwards and backwards at a scan rate of 50 mV·s^{-1} in N_2-saturated 0.5 M H_2SO_4 solution. Such a potential range for accelerated degradation tests should enlighten any problem related to the corrosion of carbon supports as well as the sintering of Pt nanoparticles based on the protocol suggested by DoE [53].

4. Conclusions

In this work a C-MnO$_2$ hybrid support was coated with platinum nanoparticles followed by a annealing at 600 °C, in order to promote the methanol oxidation reaction. The enhancement of the electrochemical performance of the Pt/C-Mn$_x$O$_{1+x}$ was mainly due to the optimized dispersion and smaller particle size of Pt nanoparticles favored by the presence of a mixture of Mn$_2$O$_3$ and Mn$_3$O$_4$,

as well as synergistic integration of nanomaterials. Pt/C-Mn$_x$O$_{1+x}$ shows better activity than the commercial Pt/C catalyst. However, its performance still falls short of the most commonly used commercial PtRu/C catalyst, due to the presence of some Pt agglomerates. The aspiration that this hybrid support can be optimized and then go on to replace the current PtRu based catalysts can be realized by understanding the real function of this kind of hybrid support and by reducing the presence of Pt agglomerates. All results suggested that the Pt/C-Mn$_x$O$_{1+x}$ can act as promising catalysts for fuel cells.

Author Contributions

A.H.A.M.V. and L.O. conceived and designed the experiments; L.O. and R.A.M.E. performed the experiments; J.Z. and C.F. prepared and characterized the catalysts; A.H.A.M.V., L.O., and S.S. analyzed data, wrote and revised the paper.

Conflicts of Interest

The authors declare no conflict of interest.

References

1. Specchia, S.; Francia, C.; Spinelli. P. Polymer Eelectrolyte Membrane Fuel Cells. In *Electrochemical Technologies for Energy Storage and Conversion*, 1st ed.; Liu, R.S., Zhang, L., Sun, X., Liu, H., Zhang, J., Eds.; Wiley: Weinheim, Germany, 2010; Volume 1, pp. 601–670.
2. Sebastián, D.; Lázaro, M.J.; Moliner, R.; Suelves, I.; Aricò, A.S.; Baglio, V. Oxidized carbon nanofibers supporting PtRu nanoparticles for direct methanol fuel cells. *Int. J. Hydrogen Energy* **2014**, *39*, 5414–5423.
3. Santasalo-Aarnio, A.; Borghei, M.; Anoshkin, I.V.; Nasibulin, A.G.; Kauppinen, E.I.; Ruiz, V.; Kallio, T. Durability of different carbon nanomaterial supports with PtRu catalyst in a direct methanol fuel cell. *Int. J. Hydrogen Energy* **2012**, *37*, 3415–3424.
4. Monteverde Videla, A.H.A.; Alipour Moghadam Esfahani, R.; Peter, I.; Specchia, S. Influence of the preparation method on Pt$_3$Cu/C electrocatalysts for the oxygen reduction reaction. *Electrochim. Acta* **2015**, doi:10.1016/j.electacta.2015.02.040.
5. Gasteiger, H.A.; Kocha, S.S.; Sompalli, B.; Wagner, F.T. Activity benchmarks and requirements for Pt Pt-alloy and non-Pt oxygen reduction catalysts for PEMFCs. *Appl. Catal. B* **2005**, *56*, 9–35.

6. Cai, J.; Huang, Y.; Huang, B.; Zheng, S.; Guo, Y. Enhanced activity of Pt nanoparticle catalysts supported on manganese oxide-carbon nanotubes for ethanol oxidation. *Int. J. Hydrogen Energy* **2014**, *39*, 798–807.

7. Kulesza, P.J.; Pieta, I.S.; Rutkowska, I.A.; Wadas, A.; Marks, D.; Klak, K.; Stobinski, L.; Cox, J.A. Electrocatalytic oxidation of small organic molecules in acid medium: Enhancement of activity of noble metal nanoparticles and their alloys by supporting or modifying them with metal oxides. *Electrochim. Acta* **2013**, *110*, 474–483.

8. Mani, P.; Srivastava, R.; Strasser, P. Dealloyed binary PtM_3 (M = Cu, Co, Ni) and ternary $PtNi_3M$ (M = Cu, Co, Fe, Cr) electrocatalysts for the oxygen reduction reaction: Performance in polymer electrolyte membrane fuel cells. *J. Power Sources* **2011**, *196*, 666–673.

9. Sundarrajan, S.; Allakhverdiev, S.I.; Ramakrishna, S. Progress and perspectives in micro direct methanol fuel cell. *Int. J. Hydrogen Energy* **2012**, *37*, 8765–8786.

10. Meher, S.K.; Rao, G.R. Morphology-controlled promoting activity of nanostructured MnO_2 for methanol and ethanol electrooxidation on Pt/C. *J. Phys. Chem. C* **2013**, *117*, 4888–4900.

11. Wu, M.; Han, M.; Li, M.; Li, Y.; Zeng, J.; Liao, S. Preparation and characterizations of platinum electrocatalysts supported on thermally treated CeO_2–C composite support for polymer electrolyte membrane fuel cells. *Electrochim. Acta* **2014**, *139*, 308–314.

12. Zhou, W.; Zhou, Z.; Song, S.; Li, W.; Sun, G.; Tsiakaras, P.; Xin, Q. Pt based anode catalysts for direct ethanol fuel cells. *Appl. Catal. B* **2003**, *46*, 273–285.

13. Zhou, C.; Wang, H.; Peng, F.; Liang, J.; Yu, H.; Yang, J. MnO_2/CNT supported Pt and PtRu nanocatalysts for direct methanol fuel cells. *Langmuir* **2009**, *25*, 7711–7717.

14. Boucher, M.B.; Goergen, S.; Yi, N.; Flytzani-Stephanopoulos, M. "Shape effects" in metal oxide supported nanoscale gold catalysts. *Phys. Chem. Chem. Phys.* **2011**, *13*, 2517–2527.

15. Xu, M.W.; Bao, S.J. Nanostructured MnO_2 for electrochemical capacitor, energy storage in the emerging era of smart grids. In *Energy Storage in the Emerging Era of Smart Grids*; Carbone, R., Ed.; InTech: Rijeka, Croatia, 2011. Available online: http://cdn.intechopen.com/pdfs-wm/20372.pdf (accessed on 9 March 2015).

16. Huang, X.; Lv, D.; Yue, H.; Attia, A.; Yang, Y. Controllable synthesis of α- and β-MnO_2: Cationic effect on hydrothermal crystallization. *Nanotechnology* **2008**, *19*, 225606, doi:10.1088/0957-4484/19/22/225606.

17. Xiao, W.; Wang, D.; Lou, X.W. Shape-controlled Synthesis of MnO_2 nanostructures with enhanced electrocatalytic activity for oxygen reduction. *J. Phys. Chem. C* **2010**, *114*, 1699–1700.

18. Calderón, J.C.; Mahata, N.; Pereira, M.F.R.; Figueiredo, J.L.; Fernandes, V.R.; Rangel, C.M.; Calvillo, L.; Lázaro, M.J.; Pastor, E. Pt-Ru catalysts supported on carbon xerogels for PEM fuel Cells. *Int. J. Hydrogen Energy* **2012**, *37*, 7200–7211.

19. Fu, X.Z.; Liang, Y.; Chen, S.P.; Lin, J.D.; Liao, D.W. Pt-rich shell coated Ni nanoparticles as catalysts for methanol electro-oxidation in alkaline media. *Catal. Commun.* **2009**, *10*, 1893–1897.

20. Rahsepar, M.; Pakshir, M.; Piao, Y.; Kim, H. Synthesis and electrocatalytic performance of high loading active PtRu multiwalled carbon nanotube catalyst for methanol oxidation. *Electrochim. Acta* **2012**, *71*, 246–251.

21. Woo, S.; Lee, J.; Park, S.K.; Kim, H.; Chung, T.D.; Piao, Y. Enhanced electrocatalysis of PtRu onto graphene separated by Vulcan carbon spacer. *J. Power Sources* **2013**, *222*, 261–266.

22. Wang, Z.B.; Yin, G.P.; Shi, P.F. The influence of acidic and alkaline precursors on Pt-Ru/C catalyst performance for a direct methanol fuel cell. *J. Power Sources* **2007**, *163*, 688–694.

23. Ban, S.; Malek, K.; Huang, C. A molecular simulation study of Pt stability on oxidized carbon nanoparticles. *J. Power Sources* **2013**, *221*, 21–27.

24. Han, B.; Zhang, F.; Feng, Z.; Liu, S.; Deng, S.; Wang, Y.; Wang Y. A designed Mn_2O_3/MCM-41 nanoporous composite for methylene blue and rhodamine B removal with high efficiency. *Ceram. Int.* **2014**, *40*, 8093–8101.

25. Moses Ezhil Raj, A.; Grace Victoria, S.; Bena Jothy, V.; Ravidhas, C.; Wollschläger, J.; Suendorf, M.; Neumann, M.; Jayachandran, M.; Sanjeeviraj, C. XRD and XPS characterization of mixed valence Mn_3O_4 hausmannite thin films prepared by chemical spray pyrolysis technique. *Appl. Surf. Sci.* **2010**, *256*, 2920–2926.

26. Julien, C.M.; Massot, M.; Poinsignon, C. Lattice vibrations of manganese oxides Part I. Periodic structures. *Spectrochim. Acta A* **2004**, *60*, 689–700.

27. Stobbe, E.R.; de Boer, B.A.; Geus, J.W. The reduction and oxidation behaviour of manganese oxides. *Catal. Today* **1999**, *47*, 161–167.

28. Baturina, O.A.; Aubuchon, S.R.; Wynne, K.J. Thermal stability in air of Pt/C catalysts and PEM fuel cell catalyst layers. *Chem. Mater.* **2006**, *18*, 1498–1504.

29. Zamanzad Ghavidel, M.R.; Bradley Easton, E. Thermally induced changes in the structure and ethanol oxidation activity of $Pt_{0.25}Mn_{0.75}$/C. *Appl. Catal. B* **2015**, *176–177*, 150–159.

30. Liu, H.X.; Tian, N.; Brandon, M.P.; Zhou, Z.Y.; Lin, J.L.; Hardacre, C.; Lin, W.F.; Sun, S.G. Tetrahexahedral Pt nanocrystal catalysts decorated with Ru adatoms and their enhanced activity in methanol electrooxidation. *ACS Catal.* **2012**, *2*, 708–715.

31. Li, L.; Xing, Y. Pt-Ru nanoparticles supported on carbon nanotubes as methanol fuel cell catalysts. *J. Phys. Chem. C* **2007**, *111*, 2803–2808.

32. Kang, Y.; Murray, C.B. Synthesis and electrocatalytic properties of cubic Mn-Pt nanocrystals (Nanocubes). *J. Am. Chem. Soc.* **2010**, *132*, 7568–7569.

33. Yang, X.; Wang, X.; Zhang, G.; Zheng, J.; Wang, T.; Liu, X.; Shu, C.; Jiang, L.; Wang, C. Enhanced electrocatalytic performance for methanol oxidation of Pt nanoparticles on Mn_3O_4-modified multi-walled carbon nanotubes. *Int. J. Hydrogen Energy* **2012**, *37*, 11167–11175.

34. Xu, C.; Shen, P.K. Electrochemical oxidation of ethanol on Pt-CeO_2/C catalysts. *J. Power Sources* **2005**, *142*, 27–29.

35. Zeng, J.; Francia, C.; Gerbaldi, C.; Baglio, V.; Specchia, S.; Aricò, A.S.; Spinelli, P. Hybrid ordered mesoporous carbons doped with tungsten trioxide as supports for Pt electrocatalysts for methanol oxidation reaction. *Electrochim. Acta* **2013**, *94*, 80–91.

36. Alegre, C.; Gálvez, M.E.; Baquedano, E.; Pastor, E.; Moliner, R.; Lázaro, M.J. Influence of support's oxygen functionalization on the activity of Pt/carbon xerogels catalysts for methanol electro-oxidation. *Int. J. Hydrogen Energy* **2012**, *37*, 7180–7191.

37. Maillard, F.; Schreier, S.; Savinova, E.R.; Weinkauf, S.; Stimming, U. Influence of particle agglomeration on the catalytic activity of carbon-supported Pt nanoparticles in CO monolayer oxidation. *Phys. Chem. Chem. Phys.* **2005**, *7*, 385–393.

38. Wang, H.; Abruña, H.D. Origin of multiple peaks in the potentiodynamic oxidation of CO adlayers on Pt and Ru-modified Pt electrodes. *J. Phys. Chem. Lett.* **2015**, *6*, 1899–1906.

39. Meher, S.K.; Rao, G.R. Polymer-assisted hydrothermal synthesis of highly reducible shuttle-shaped CeO_2: Microstructural effect on promoting Pt/C for methanol electrooxidation. *ACS Catal.* **2012**, *2*, 2795–2809.

40. Wei, Z.D.; Ji, M.B.; Hong, Y.; Sun, C.X.; Chan, S.H.; Shen, P.K. MnO_2–Pt/C composite electrodes for preventing voltage reversal effects with polymer electrolyte membrane fuel cells. *J. Power Sources* **2006**, *160*, 246–251.

41. Lee, S.W.; Chen, S.; Sheng, W.; Yabuuchi, N.; Kim, Y.-T.; Mitani, T. Roles of surface steps on Pt nanoparticles in electro-oxidation of carbon monoxide and methanol. *J. Am. Chem. Soc.* **2009**, *131*, 15669–15677.

42. Gong, X.; Yang, Y.; Huang, S. Mn_3O_4 catalyzed growth of polycrystalline Pt nanoparticles and single crystalline Pt nanorods with high index facets. *Chem. Commun.* **2011**, *47*, 1009–1011.

43. Aricò, A.S.; Srinivasan, S.; Antonucci, V. DMFCs from fundamental aspects to technology development. *Fuel Cells* **2001**, *1*, 133–161.

44. Velázquez-Palenzuela, A.; Centellas, F.; Garrido, J.A.; Arias, C.; Rodríguez, R.M.; Brillas, E.; Cabot, P.L. Kinetic analysis of carbon monoxide and methanol oxidation on high performance carbon-supported Pt–Ru electrocatalyst for direct methanol fuel cells. *J. Power Sources* **2011**, *196*, 3503–3512.

45. Raoof, J.B.; Ojani, R.; Hosseini, S.R. Electrochemical fabrication of novel Pt/poly (m-toluidine)/Triton X-100 composite catalyst at the surface of carbon nano-tube paste electrode and its application for methanol oxidation. *Int. J. Hydrogen Energy* **2011**, *36*, 52–63.

46. Ye, K.-H.; Zhou, S.-A.; Zhu, X.-C.; Xu, C.-W.; Shen, P.K. Stability analysis of oxide (CeO_2, NiO, Co_3O_4 and Mn_3O_4) effect on Pd/C for methanol oxidation in alkaline medium. *Electrochim. Acta* **2013**, *90*, 108–111.

47. Mao, L.; Zhang, K.; Chan, H.S.O.; Wu, J.S. Nanostructured MnO_2/graphene composites for supercapacitor electrodes: The effect of morphology, crystallinity and composition. *J. Mater. Chem.* **2012**, *22*, 1845–1851.

48. Trogadas, P.; Ramani, V. Pt/C/MnO_2 hybrid electrocatalysts for degradation mitigation in polymer electrolyte fuel cells. *J. Power Sources* **2007**, *174*, 159–163.

49. Huang, H.; Chen, Q.; He, M.; Sun, X.; Wang, X. A ternary Pt/MnO_2/graphene nanohybrid with an ultrahigh electrocatalytic activity toward methanol oxidation. *J. Power Sources* **2013**, *239*, 189–195.

50. Aricò, A.S.; Baglio, V.; di Blasi, A.; Modica, E.; Antonucci, P.L.; Antonucci, V. Analysis of the high-temperature methanol oxidation behaviour at carbon-supported Pt–Ru catalysts. *J. Electroanal. Chem.* **2003**, *557*, 167–176.

51. Garsany, Y.; Ge, J.; St-Pierre, J.; Rocheleau, R.; Swider-Lyons, K.E. Analytical procedure for accurate comparison of rotating disk electrode results for the oxygen reduction activity of Pt/C. *J. Electrochem. Soc.* **2014**, *161*, F628–F640.

52. Sneed, B.T.; Young, A.P.; Jalalpoor, D.; Golden, M.C.; Mao, S.; Jiang, Y.; Wang, Y.; Tsung, C.K. Shaped PdNiPt core-sandwich-shell nanoparticles: Influence of Ni sandwich layers on catalytic electrooxidations. *ACS Nano* **2014**, *7*, 7239–7250.

53. US DoE 2014 Annual Progress Report V. Fuel Cells. Available online: http://www.hydrogen. energy.gov/annual_progress14_fuelcells.html#a (accessed on 12 January 2015).